Molecular dynamics for irradiation driven chemistry
application to the FEBID process

Sushko, Gennady B.; Solov'yov, Ilia A.; Solov'yov, Andrey V.

Published in:
European Physical Journal D. Atomic, Molecular, Optical and Plasma Physics

DOI:
10.1140/epjd/e2016-70283-5

Publication date:
2016

Document version:
Accepted manuscript

Citation for pulished version (APA):
Sushko, G. B., Solov'yov, I. A., & Solov'yov, A. V. (2016). Molecular dynamics for irradiation driven chemistry: application to the FEBID process. *European Physical Journal D. Atomic, Molecular, Optical and Plasma Physics*, *70*, 217-231. https://doi.org/10.1140/epjd/e2016-70283-5

EPJ manuscript No.
(will be inserted by the editor)

Molecular dynamics for irradiation driven chemistry: application to the FEBID process

Gennady B. Sushko[1], Ilia A. Solov'yov[2,3a], Andrey V. Solov'yov[1,3]

[1] MBN Research Center, Altenhöferallee 3, 60438 Frankfurt am Main, Germany
[2] University of Southern Denmark (SDU), Campusvej 55, 5230, Odense M, Denmark
[3] On leave from A.F. Ioffe Physical-Technical Institute Russian Academy of Sciences, Polytekhnicheskaya st. 26, 194021 St. Petersburg, Russia

the date of receipt and acceptance should be inserted later

Abstract. A new molecular dynamics (MD) approach for computer simulations of irradiation driven chemical transformations of complex molecular systems is suggested. The approach is based on the fact that irradiation induced quantum transformations can often be treated as random, fast and local processes involving small molecules or molecular fragments. We advocate that the quantum transformations, such as molecular bond breaks, creation and annihilation of dangling bonds, electronic charge redistributions, changes in molecular topologies, etc, could be incorporated locally into the molecular force fields that describe the classical MD of complex molecular systems under irradiation. The proposed irradiation driven molecular dynamics (IDMD) methodology is designed for the molecular level description of the irradiation driven chemistry. The IDMD approach is implemented into the MBN Explorer software package capable to operate with a large library of classical potentials, many-body force fields and their combinations. IDMD opens a broad range of possibilities for modelling of irradiation driven modifications and chemistry of complex molecular systems ranging from radiotherapy cancer treatments to the modern technologies such as focused electron beam deposition (FEBID). As an example, the new methodology is applied for studying the irradiation driven chemistry caused by FEBID of tungsten hexacarbonyl $W(CO)_6$ precursor molecules on a hydroxylated SiO_2 surface. It is demonstrated that knowing the interaction parameters for the fragments of the molecular system arising in the course of irradiation one can reproduce reasonably well experimental observations and make predictions about the morphology and molecular composition of nanostructures that emerge on the surface during the FEBID process.

1 Introduction

There are many examples in which chemical transformations of complex molecular systems are driven by irradiation. Often such modifications carry important outcomes to the functional properties of the irradiated molecular systems. Enough to mention the radiobiological phenomena, in which living cells can be inactivated by irradiation due to the induced DNA complex strand breaks [1, 2], the formation and composition of cosmic ices and dusts in the interstellar medium and planetary atmospheres is largely a result of the interplay of the molecular surface adsorption and surface irradiation [3], the formation of biologically relevant molecules under extreme conditions involving irradiation [4][1], and many more. Irradiation driven chemistry is nowadays utilized in modern nanotechnology, such as focused electron beam deposition (FEBID) [5, 6] and extreme ultraviolet lithography (EUVL) [7, 8]. These technologies belong to the next generation of nanofabrication techniques allowing the controlled creation of nanostructures with nanometer resolution which is attractive in both, basic and applied research. The fabrication of smaller and smaller structures has been the goal of the electronics industry for more than three decades and still remains one of this industry's biggest challenges. Furthermore, irradiation chemistry is a key element in nuclear waste decomposition technologies [9] and medical radiotherapies [1, 2].

Irradiation driven chemistry (IDC) is based on the quantum transformations that are induced in molecular systems by their irradiation by external fields of different modality (X-rays, lasers, electrons/positrons, ions, etc) and the dynamics of molecular system which can be also influenced by external factors like temperature, pressure, external fields, etc. Highly perturbed dynamical molecular systems can only be described from first principles within the time dependent density functional theory (TDTDFT), or any of its equivalents, if the size of the molecular system is sufficiently small, typically hundreds of atoms [10–14].

[a] E-mail: ilia@sdu.dk

[1] see COST Action "The Chemical Cosmos: Understanding Chemistry in Astronomical Environments" www.cost.eu/COST_Actions/cmst/CM0805

This strong limitation makes TDDFT of limited use for the description of the IDC of complex molecular systems.

Classical molecular dynamics (MD) could be considered as an alternative for the theoretical description of IDC. Nowadays, the MD simulation of atomic and molecular systems of various sizes, materials and properties is possible. For instance, by employing the classical molecular dynamics (often also called mechanics) approach it is at present feasible to study structure and dynamics of molecular systems that are constituted of millions of atoms [15, 16] and evolve on time scales up to hundreds of nanoseconds [17, 18]. In the molecular mechanics approach, the molecular system is treated classically, i.e., the atoms of the system are interacting with each other through a parametric phenomenological potential, that is governed by the type of the individual atoms and by the network of the chemical bonds between them. This network defines the so-called molecular topology, i.e., a set of rules that impose constraints on the system, and permit maintaining its natural shape, as well as its mechanical and thermodynamical properties. The molecular mechanics method has been widely used throughout the last decades [14, 16, 19–21, **?**–21, **?**–21], and has, for example, been implemented in the well established computational packages CHARMM [22], AMBER [23], GROMACS [24] and NAMD [25].

In spite of the manyfold advantages, classical MD is inapplicable for simulations of chemical reactions and IDC processes, because it does neither account for coupling of the molecular system to radiation, nor does it describe quantum transformations in the molecular system induced by the irradiation. In this investigation we overcome these deficiencies of MD and suggest a new methodology for simulation of irradiation driven chemical transformations of complex molecular systems. We propose to model irradiation induced quantum transformations in a molecular system as random, fast and local processes involving small molecular fragments (typically on sub-nanometer scale) of the entire system. The modeled transformations include molecular bond breakages, saturation of dangling bonds, chemical reactions in the system, and changes in the molecular topology of the system. These transformations are introduced according to the specific rates that are coupled to the irradiation field and the probabilities of the corresponding quantum processes are established through *ab initio* quantum approaches, such as many-body theory, DFT, collision theory, or taken from experiments. The fundamental basis for such an approach relies on the Born-Oppenheimer theory justifying uncoupling of the fast electronic motion in molecular systems from the slow motion of the ionic subsystem and the fact that the characteristic time scale for the fast quantum transformations in the system is typically within the femtosecond range, i.e., about the duration of one time step in MD simulations. Furthermore, the spatial dimension of the region where an irradiation induced quantum transformation take place is much smaller than the size of the molecular systems under consideration. Therefore, if the outcomes of the quantum transformations are properly accounted for on the basis of quantum mechanics or simply taken from experiment and correctly embedded as random and local modifications of the classical force fields, it becomes feasible to model structure and dynamics of large molecular systems under irradiation through the irradiation driven molecular dynamics (IDMD), as proposed in this work. This methodology is designed for the molecular level description of the irradiation driven chemistry of complex molecular systems arising in various circumstances introduced above.

The IDMD approach was implemented into the MBN Explorer software package [26] capable to operate with a large library of classical potentials, many-body force fields (including the recently implemented reactive CHARMM force field [27]) and their combinations. The MBN Explorer program[2] [26, 28, 29] is an advanced software package for complex biomolecular, nano- and mesoscopic system simulations. It is suitable for classical molecular dynamics, Monte Carlo [30–34] and relativistic dynamics simulations [35–38] of a large range of molecular systems, such as nano- [39, 40] and biological systems, nanostructured materials [41, 42], composite/hybrid materials [43–46], gases, liquids, solids and various interfaces [47, 48], with sizes ranging from atomic to mesoscopic. Among applications of MBN Explorer are also the simulations of thermo-mechanical damage in biological systems, e.g. DNA nucleosomes, caused by the propagation of shock waves induced by the propagation of ions [49, 50]. The results of such simulations are essential for the evaluation of ion-induced radiobiological effects [51] within the framework of a multiscale approach to the physics of radiation damage [52], and can be utilized for the treatment planning in the ion-beam cancer therapy [52].

There are many unique features of MBN Explorer. Thus, in the recent paper [27] the implementation of the reactive CHARMM force field in MBN Explorer was reported. This force field allows simulation of processes involving rupture and formation of covalent bonds in biomolecular systems. The standard CHARMM force field extension [53–55] takes into account additional parameters, such as dissociation energy of bonds, bond multiplicity and atom valences. The functional form of the interatomic interactions is adjusted to account for the finite value of the dissociation energy of chemical bonds.

The present implementation of IDMD in MBN Explorer opens a broad range of possibilities for modelling of irradiation driven modifications and chemistry of complex molecular systems. In order to highlight these possibilities here we present an exemplary case study of the FEBID process simulated by means of IDMD. The results of these simulations are thoroughly examined and compared with experiment.

The FEBID case study has been selected due to it importance and potentially high impact. In recent years the FEBID process was actively investigated by a broad international community represented by the European COST Action CELINA[3]. The FEBID based technology is being developed for controllable and reproducible fabrication of

[2] www.mbnexplorer.com

[3] http://www.cost.eu/COST_Actions/cmst/CM1301

surface nanostructures with high resolution below 10 nm. It is competing with the conventional nanolithographic techniques [5].

Simulations of the FEBID process and the growth of nanostructures have been performed so far using the Monte-Carlo approach and the diffusion theory. These methods allow simulations of the average characteristics of the process such as the chemical composition and the growth rate of the adsorbed nanostructures but do not provide any molecular level details of the adsorbed material, e.g. the characterisation of its crystalline or amorphous structure. The IDMD approach goes beyond this limit and provides a description of the nanostructures created by the FEBID process on the atomistic level accounting for the quantum and chemical transformation of the adsorbed molecular system being under focused electron beam irradiation.

Computational modeling of such complex molecular processes as FEBID is inevitably coupled with some approximations and modelling assumptions. This concerns the justification of the implemented computational model and the choice of its parameters. Therefore, it is important to validate the outcomes of the simulations through comparison with experiment. We perform such validation in our work for the adsorption on a hydroxylated SiO_2 surface employing the precursor tungsten hexacarbonyl and its irradiation with a focused electron beam. Experimentally this process has been studied in an earlier investigation [56].

2 Irradiation Driven Molecular Dynamics

Classical molecular dynamics (MD) has been introduced for the description of quantum molecular systems with the use of the classical Newtonian equations [22]. The justification of this approach is based on the Born-Oppenheimer theorem, which separates the light electronic and heavy ionic subsystems and elucidates the quasiclassical motion of the nuclei in the system. In this approach all the information about the quantum-mechanical properties of the system is included in the parameters of the classical force fields guiding the motion of the nuclei. Within the classical MD the trajectories of atoms and molecules are determined through the numerical solution of Newton's equations, where forces between the particles and their potential energies are calculated using interatomic potentials and force fields. Such a simplification of the description of motion of a quantum system provides significant advantages for computer simulations. With modern supercomputers, the conventional classical all atom MD simulations permit nowadays studying molecular systems up to micrometers in size on time scales up to microseconds and beyond [16, 19–21, 57]. The method was originally developed within the field of theoretical physics in the late 1950s [58] but is applied today mostly in chemical physics, materials science and the modelling of biomolecules.

The classical MD approach does not describe the electron dynamics and, therefore, most of the quantum transformations that may occur during the system dynamics. These transformations are often induced in the system through exposure to external perturbations such as external fields or irradiation by charged particles (electrons, protons, ions, etc) or photons. The resulting effects may have a global character (electric current, spin ordering, polarisation, magnetisation, etc) or be local (atomic or molecular excitation, ionisation, dissociation, charge transfer, etc). Below, we focus on the analysis of the latter case.

Irradiation induced local quantum perturbations of a molecular system typically occur on the sub-femtosecond time scale and involve only those atoms that are directly affected by the irradiation. This results in the creation of secondary electrons, ions, reactive species (radicals), and excited molecules, which can further interact with the molecular system and cause further chemical transformations. This complex local dynamics typically involves the nearest environment of the targeted molecular site, being a small part of the entire molecular system, and is completed within femtoseconds. During this time some of the initial perturbations of the system, such as quasi-free electrons, electron holes, ionic charges, relax and vanish, due to the high electronic mobility and the Coulomb attraction. The femtosecond time scale is, however, still significantly shorter than the characteristic timescales responsible for the motion of the entire molecular system. Indeed, in classical MD a typical integration time step is 1-2 fs, corresponding to the oscillation period of a hydrogen atom at room temperature.

The notable outcome of the process described above is the emergence of bond breaks in the system. These events are most significant as they affect the dynamical behaviour and chemical transformations in the molecular system on the larger time scales, up to nanoseconds and beyond, being the typical time frame for the classical MD. The bond breaks arise in those parts of the molecular system which are targeted by the irradiation. They occur randomly with a probability depending on the intensity and the modality of irradiation. The probabilities of these events are related to the cross sections of the involved irradiation induced processes (elastic and inelastic scattering, electronic and vibrational excitation, dissociative electron attachment, collision dissociation, etc) occurring in the system on the femtosecond time scale and can be elaborated from the collision theory or be taken from experiment.

Irradiation conditions for a molecular system can differ substantially and depend on the radiation modality, duration of the system exposure to irradiation and the system geometry. Irradiation can be a swift single event, like a single ion track crossing the molecular system, or it can last a certain period of time up to some nanoseconds and even longer. In the latter case the irradiation induced bond breaks and charge redistribution in the system occurs during the entire irradiation period. Irradiation can be homogeneous within a certain volume or strongly inhomogeneous. The choice of the irradiation conditions corresponds to each particular case study. In the follow up sections we consider these for the FEBID process.

The above described scenario defines the irradiation driven molecular dynamics (IDMD). The IDMD can be

introduced as classical MD with the superimposed random process of molecular bond breakage related to the irradiation conditions. The bond breakage is defined as the local alteration of the system force fields, which involves (i) creation of reactive atomic species (radicals) with dangling bonds, (ii) the possibility of dangling bonds' closure and creation of new molecular bonds or molecules, (iii) accounting for molecular topology changes (in the cases when it is defined, e.g. molecular mechanics force fields). The characterisation of these modifications of the classical MD force fields can be elaborated on the basis of quantum chemistry methods. Examples of such characterisation for the FEBID process are given below.

The proposed methodology aims to account for the major dissociative transformations of the molecular system induced by its irradiation and possible paths of further reactive transformations. The latter are sensitive to statistical mechanical factors, like the concentration of the reactive spices, their mobility (diffusion), the temperature of the medium, etc. All these factors are automatically accounted for in a correct way through the Langevin MD describing the molecular system as a NVT statistical mechanics ensemble. The local deviations from the statistical mechanics equilibrium arising in the vicinity of the breaking bonds caused by the local deposition of energy into the system leads to minor perturbations of the large molecular system and can be incorporated into IDMD as a perturbation.

The concept of IDMD is general and applicable to any kind of molecular system treated with any type of classical force field. The method is implemented in the MBN Explorer software package [26] and can operate with the large library of force fields implemented in MBN Explorer. In its current realisation IDMD is capable to describe systems modeled through pairwise potentials, many-body force fields, molecular mechanics force fields (including the recently implemented reactive CHARMM force field [27]) and their combinations. The limited number of parameters that determine molecular force fields, and their irradiation driven perturbations, results in a countable number of modifications that could occur in a molecular system upon irradiation and makes the method efficient and accurate. This implementation opens a broad range of possibilities for modelling of irradiation driven modifications and chemistry of complex molecular systems.

Below we provide the validation of the introduced IDMD methodology through the simulation of the FEBID process, detail analysis of the results obtained and their comparison (where possible) with the results of the Monte Carlo approach and experiment.

3 Modeling of FEBID with IDMD

In FEBID a previously adsorbed molecular precursor is dissociated in the focus of an electron beam typically provided by a scanning or transmission electron microscope. The FEBID process can be modelled with the aid of IDMD at the atomistic level of detail. The exemplary study presented below deals with the irradiation driven chemistry of tungsten hexacarbonyl $W(CO)_6$ on a SiO_2 surface. The details of modelling of the FEBID and irradiation processes with IDMD are described and the choice of parameters is justified.

3.1 FEBID process

Let us now apply the IDMD modelling approach to the growth process of the W enriched nanostructure in the course of the adsorption of $W(CO)_6$ precursor molecules on a hydroxylated SiO_2 surface and their repetitive irradiation with an electron beam.

The process starts with the initial adsorption of precursor over the surface. In the model considered all the atoms in the precursor are moving, while substrate atoms on which the precursor adsorbs are considered fixed. Typically the initial adsorption leads to the formation of precursor monolayer or a part of it. The W-containing nanostructure growth over the surface is modeled then through a series of subsequent simulations where the results of each simulation are used as input for the following one. Each round of simulations is divided into two phases: precursor adsorption phase and irradiation phase; Fig. 1 illustrates this idea.

During the irradiation phase all the molecules in the system, except atoms of the substrate, are moving. During this period (although typically lasting in experiment from microseconds to milliseconds, see discussion below) simulated up to nanoseconds, it is assumed that the random dissociation of the W–(CO) bonds in the precursor molecules occurs resulting in the emergence of reactive molecular fragments (including free W atoms) with dangling bonds. Within the model, the CO molecules emerge in the system solely during the dissociation of the precursor molecules and its fragments and cannot undergo any further degradation. The dynamics and interaction of the fragments may lead to the formation of new bonds between W atoms and their coalescence into W enriched islands (clusters) with either crystalline like or amorphous structures depending on the model for the W-W binding. Two models for the W chemistry are considered. The model A describes growth of the nanostructure without restructuring of the bonds (W-W, W-C, C-C) inside the W-enriched nanostructure. This model accounts for the chemistry of precursors newly added to the system without restructuring of the open bonds within the growing nanostructures. The model B accounts for the formation of new bonds inside the growing nanostructures. In both models the W-(CO) bond breaking in precursors is described using the dissociative force field implemented in MBN Explorer [27] and accounting for the dynamically changing molecular topology of a system within the classical molecular mechanics framework. The dissociative force field also takes into account additional parameters of the system, such as the dissociation energy of chemical bonds, bonds multiplicity and the valence of atoms. Atomic valencies define the maximal number of covalent bonds for

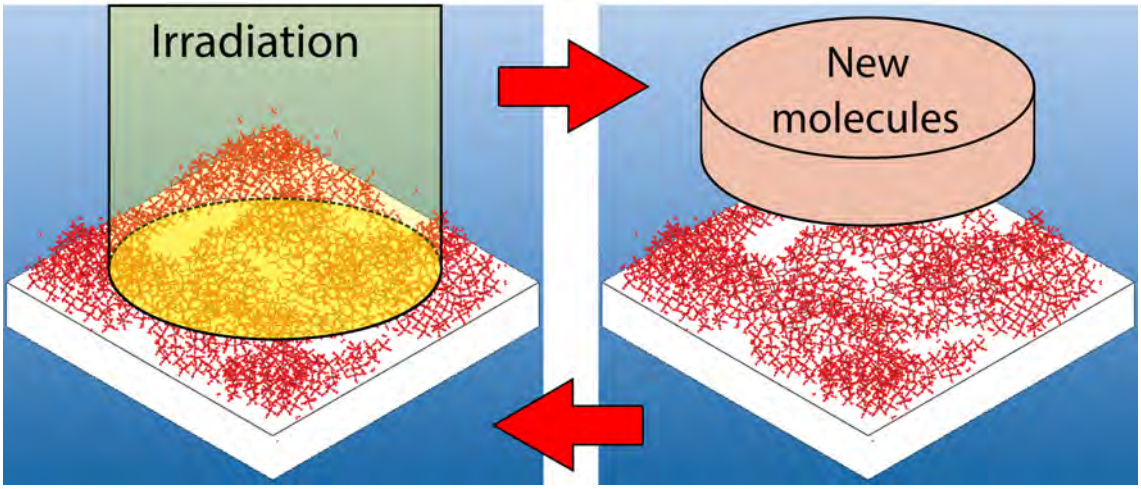

Fig. 1. Schematic illustration of the simulation protocol used for modeling of the FEBID process. At the initial stage a number of molecules are randomly dispersed over the surface forming nearly a monolayer. Then simulation is performed as a repetitive process. Each stage of the process consists of the two phases: (i) random adsorption of new precursor molecules atop the surface of emerging nanostructure and (ii) exposure of the system to radiation. The irradiation/adsorption phases interchange continuously during the entire span of the simulation.

each atom type, while each bond is also allowed to have a certain multiplicity value to mimic the effect of single, double, triple bonds. It is, thus required that for each atom, the sum of its bond multiplicities does not exceed the valency value. The concrete choice of the parameters for the dissociative force field is described below. Irradiation of precursor molecules leads to occasional formation of CO molecules in the system. These molecules remain in the simulation box until the end of the current irradiation phase and are removed thereafter. This accounts for their desorption from the surface and equilibration in the entire large volume of the system.

The irradiation phase is followed by the adsorption phase during which a layer of precursor molecules is added to the system to account for the adsorption of precursor molecules from the gas phase. In experiment this phase lasts typically some milliseconds or even longer, being a rather long period for the direct MD simulations. The adsorption process, however, can be modelled using the multiscale simulations based on the combined use of MD and Monte-Carlo (MC) approaches [32, 33].

In this work the adsorption phase modelling is simplified and reduced to the random addition of a certain number of new precursor molecules atop the already existing surface of the molecular structure with the following relaxation of the whole system. This approach allows avoiding MD simulation of the deposition process of precursor molecules from the gas phase and, therefore, to bypass the related difficulties in simulating molecules at low pressure and temperature. The relaxation is needed for improving the binding of newly adsorbed molecules to the already existing surface molecular structure. Due to the weak interaction between precursors, the molecules which are landed on the surface atop of precursors at the room temperature tend to evaporate during the irradiation phase. This explains the finite and practically constant thickness of the layer of precursor molecules outside the region of irradiation, while inside the region newly adsorbed molecules typically get attached to the growing nanostructure.

The irradiation and adsorption phases can be characterised by the irradiation time τ_d (dwell time) and by the time interval between individual irradiations τ_r (replenishment time). Typically, they are significantly different, $\tau_r \gg \tau_d$. The shortest period of τ_d discussed in literature [6] is $\tau_d \sim 1$ ns, while $\tau_r \sim 2$ ms. Thus the value of $\tau_d = 10$ ns and $\tau_r = 2$ ms are chosen in the simulations reported here.

The $W(CO)_6$ precursor molecules are added to the system at the conditions close to experimental [56]. Thus at the experimental precursor gas pressure $P = 0.330$ Pa the flux of precursor molecules towards the surface is $F = 2.7 \cdot 10^3$ 1/nm^{2}s.

Computations were carried out in a simulation box with reflective boundary conditions having the dimensions of 14 nm $\times$ 14 nm $\times$ 48 nm with the longer side of the box directed perpendicular to the SiO_2 surface, which is placed at the bottom of the simulation box. The size of the simulation box was chosen to reduce the possible artificial impact of the emerging CO molecules on the nanostructure growth in the course of the irradiation phase. The box size was established through a series of test simulations. At the chosen size the influence of the CO molecules is negligible.

The parameters outlined above allow to estimate the number of $W(CO)_6$ molecules incoming into the simulation box during the replenishment time as 1060, for the dwell time this number becomes negligibly small, i.e. much smaller than 1. Due to the low binding energy between precursor molecules only one layer of molecules is adsorbed on the surface and most of the molecules adsorbed outside of the irradiated area get not attached to the surface. The irradiated area is defined by the beam of radius of 5 nm

which would thus result in 424 molecules per adsorption phase.

The surface occupied by one precursor can be estimated through its radius (3.2Å), which gives a value of 0.3 nm^2. However, each precursor occupies a larger area on the surface due to the finite distance between the precursors and the type of their packing. In simulations the maximum, optimized average area per precursor is found to be equal to 0.4 nm^2. In the paper [55] it is reported as 1.4 nm^2. With 0.4 nm^2 surface area per precursor one can place up to 196 molecules within the irradiated area. In simulations approximately two-fold smaller number is used and thus 100 new molecules per adsorption phase in the area above the irradiation spot get adsorbed.

The estimates indicate that (i) during the irradiation phase the appearance of new precursor molecules is negligibly small; (ii) the number of precursor molecules that emerge during the replenishment time is sufficient to form a monolayer atop the already existing nanostructure on the surface; these molecules are dispersed randomly over the surface after each completed irradiation phase. Finally note that due to the low binding affinity between precursor molecules the number of precursor layers that can be kept on the surface is limited. Thus, only some of the newly adsorbed precursors remain on the surface.

3.2 Irradiation process

A snapshot of MD simulation of the first irradiation phase described above is shown in Fig. 2. The interaction of precursor molecules with the cylindrical electron beam depicted in green leads to the precursor fragmentation and the formation of W clusters on the surface, illustrated in Fig. 2 in blue. Let us now discuss this irradiation process in details.

The direct interaction of the primary electrons (PE) of the beam with precursor molecules and the surface generates the secondary electrons (SE) in the adsorbed medium, as well as the backscattered electrons (BSE). The secondary and backscattered electrons increase the probability of molecular bond dissociation and the effective beam radius. These processes and their influence on the surface nanostructure growth were studied earlier numerically [59, 60]. In the earlier investigation [56] it was demonstrated that the cumulative action of SE and BSE electrons leads to a 40-fold increase of the yield of tungsten as compared to the action of just the PE. This factor depends on the accelerating voltage of the beam, the properties of the surface and other factors.

In the present study the irradiation process is considered for an electron beam of the cylindrical shape with a given radius, see Fig. 2. Only those precursors that move inside the cylinder are exposed to radiation and may dissociate, while molecules outside the cylinder are not affected by irradiation. The dissociation rate of the precursor molecules can be evaluated from the reported experimental yield of tungsten atom per electron [56]. Note that this approach does not take into account the influence of the emerging tungsten nanostructure on the SE production which might become essential for the evaluation of the precursor dissociation rate in the vicinity of a thicker tungsten nanostructure. The dissociation of precursors could also be obtained on the basis of the quantum collision theory coupled to the description of electron transport through the system. This description, however, goes beyond the scope of this paper.

In the simulations reported below the characteristics correspond to those used in [56]. In that paper the energy of primary electrons was taken as $V = 30$ keV, the beam current $I_0 = 79$ pA, the beam radius $R = 10$ nm, the irradiation time $\tau_d = 1$ ms. At present it is impossible to perform MD simulations on the millisecond timescale. Therefore, the FEBID process is modelled at the rescaled computationally accessible parameters that preserve the number of electrons targeting the system (electron fluence) and thus producing the irradiation driven effects on the same scale as in experiment. Thus, the irradiation time in simulations has been decreased, while the beam currents are increased. Specifically, the beam accelerating voltage is chosen equal to $V = 30$ keV, the dwell time to $\tau_d = 10$ ns, the beam current to $I_0 = 4$ μA, and the beam radius to 5 nm. These numbers define a reference case study with which other sets of simulation parameters are compared. These parameters set up the electron fluence per dwell time equal to $N_e = 2.5 \times 10^5$ electrons, while in experiment [56] the electron fluence per dwell time was $N_e = 4.94 \times 10^5$, i.e. approximately two times larger than in the simulation reference case study. Due to the cross section of the beam in experiment [56] being four times larger than in the reference case simulations, the electron fluence per unit area, i.e. fluence density, in experiment ($1.57 \cdot 10^3$ nm^{-2} per dwell time) [56] was approximately two times smaller than in the reference study simulation ($3.18 \cdot 10^3$ nm^{-2} per dwell time).

Now let us analyse the probability of W-C bonds dissociation in $W(CO)_6$ caused by collisions with electrons. The probability of precursor dissociation per unit time can be evaluated as

$$P = \sigma \cdot J_0, \tag{1}$$

where σ is the bond dissociation cross section and J_0 is the electron flux density targeting the precursor. $J_0 = I_0/(e \cdot S_0)$, with I_0 being the electron beam current, e is the electron charge and S_0 is the beam cross section equal to πR^2. Substituting these relationships into Eq. (1) one derives

$$P = \frac{I_0}{e}\frac{\sigma}{S_0}, \tag{2}$$

Estimating $I_0 = 4$ μA, and $\sigma = 1.2 \cdot 10^{-2}$ nm^2 [56], one derives $P_0 = 3.82 \cdot 10^{-6}$ fs^{-1}. This number corresponds to the dissociation of 6 W-C bonds in $W(CO)_6$ in the reference case study. The probability P_{W-C} of the dissociation of a single W-C bond in $W(CO)_6$ should be comparable in the magnitude as it should corresponds to a transition to different repulsive energy term (decay channel) in $W(CO)_6$. The probability P_{W-C} becomes larger when accounting for SE and BSE emitted from the substrate. In

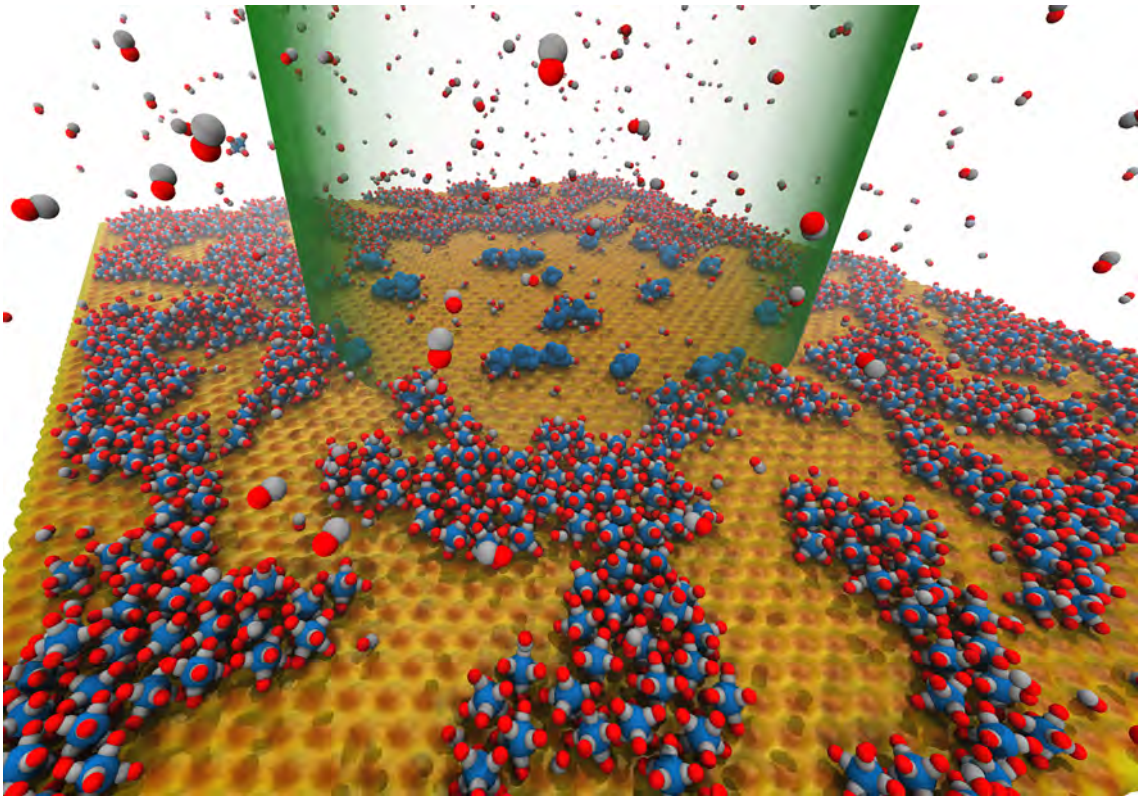

Fig. 2. Snapshot of MD simulation of adsorption of $W(CO)_6$ precursor molecules on a SiO_2 surface in the case of model A (see text) experiencing the early stage of irradiation by the electrons beam (shown as transparent green cylinder). The interaction of precursor molecules with the beam leads to fragmentation of molecules and formation of W clusters, shown in blue.

this paper we do not analyse these factors numerically and simply round the above number to the nearest order of magnitude, i.e. we estimate $P_{W-C} = 10^{-5}$ fs^{-1}. This number has been used in the reference case study simulations. For the lower electron currents with the fixed voltage V the W-C bond dissociation probability P_{W-C} is chosen according to Eq. (2) as a proportional fraction of P_{W-C}. The probability P_{W-C} depends on the voltage V, because the collision induced dissociation cross section σ, the SE and BSE yields depend on the PE collision energy. Analysis of these dependencies, as well as the production of SE and BSE goes beyond the scope of the current work and will be performed in the follow up investigations.

The probability P_0 calculated with the input numbers corresponding to the experiment [56] is equal to $5.97{\cdot}10^{-12}$ fs^{-1} and $1.89 \cdot 10^{-11}$ fs^{-1} for 25 pA and 79 pA currents, correspondingly. When multiplying it by the same empirical coefficient $P_{W-C}/P_0 = 2.62$ as in simulations one derives $P_{exp} = 4.95 \cdot 10^{-11}$ fs^{-1} for $I = 79$ pA.

The probability P_{exp} is noticeably smaller than it is used in the simulations due to the smaller values of the experimental beam currents. However, the smaller irradiation times (and larger fragmentation probabilities) used in simulations as compared to experimental ones keep the electron fluences per dwell time comparable in simulations and experiment. The cross sections of the collision induced dissociation of precursors used in simulations correspond to their experimental values, thus resulting in the similar irradiation driven outcomes in the system.

3.3 Dissociative chemistry of irradiated precursors

The structure and dynamics of irradiated $W(CO)_6$ atop the hydroxylated SiO_2 surface is modelled with the dissociative CHARMM force field of MBN Explorer, which requires specification of several parameters [27]. For the studied systems these parameters define the equilibrium bond lengths, bond stiffnesses and dissociation energies. Additionally, one has to define the dissociative chemistry of precursors including the definition of the molecular fragments and atomic valences.

The necessary interaction parameters of the dissociative force fields have been deduced from the NIST[4] [61] and OpenKIM[5] databases and are compiled in Tab. 1. In the models considered only the dissociation of the bonds W-C and W-W is permitted, while the C-O bonds are treated harmonically, i.e. non-breaking. The bond cutoff distance in Tab. 1 defines the radial criterion for bond dissociation. Once the distance between the atoms exceeds the cutoff value the bond between them is considered broken, the valences of the atoms involved are reevaluated

[4] http://webbook.nist.gov/cgi/cbook.cgi?ID=C14040110

[5] https://openkim.org/dev-kim-item/LennardJones612_Universal__MO_826355984548_001

	Bond stiffness, k, kcal/(mol Å^2)	Bond length, R_{min}, Å	Dissociation energy, E_{dis}, kcal/mol	Bond cutoff, R_{cut}, Å
W-C	467.79	1.75	39.79	4.5
W-W	683.90	2.74	158.29	5.0
C-O	620.00	1.23	-	-

Table 1. Interaction parameters for the covalent bonds in $W(CO)_6$ precursor molecules. The C-O bond is treated in the harmonic approximation, i.e., using the standard CHARMM force field, while the W-C and W-W bonds are modelled using the dissociative force field implemented in MBN Explorer [27].

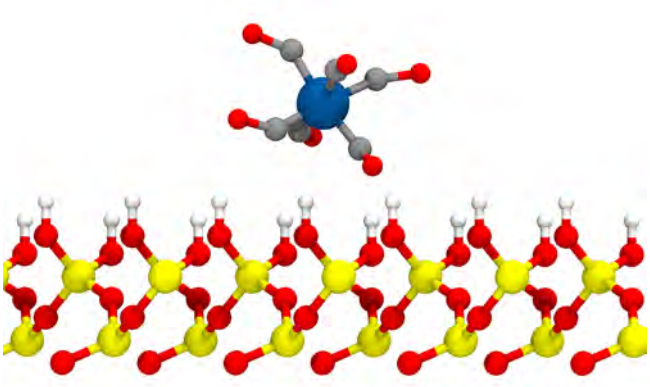

Fig. 3. Structure of the hydroxilated surface of SiO_2 with adsorbed $W(CO)_6$ precursor molecule. Yellow, red and white spheres plot Si, O, and H atoms respectively, gray and blue colors depict C and W atoms.

and the topology of the molecular system is updated. In the opposite case a chemical bond is formed when the distance between a pair of atoms with the open valency becomes smaller than the cutoff value. The breakage and formation of new chemical bonds involves also the reevaluation of the atomic types, valences, and the topology of the molecular system.

The forcefield potential that describes any chemical bond in the system converges to a zero-asymptotically at large interatomic distances. The formal formation and assignment of a new chemical bond between a pair of atoms does not affect the energy of these atoms because the bond energy is small at the bond cutoff distance. This is an algorithmic procedure that instructs MBN Explorer to check if two candidate atoms could form a chemical bond upon their encounter. In the case if the kinetic energy of atoms upon their encounter at a cutoff distance is higher than this bonded energy value, a bond would not be formed and rupture as soon as the atoms involved move further apart. In other words, a newly assigned bond will not remain in the system and will not influence the statistical results.

The interaction of precursors with the hydroxylated SiO_2 surface is modeled through the effective pairwise Lennard-Jones potentials for the interaction between the atoms of precursors and the atoms of the surface. The parameters of these interactions for W, C, Si, O and H are chosen to reproduce the total interaction energy of $W(CO)_6$ with hydroxylated SiO_2, being ~ 0.8 eV. DFT calculations [62] report the energy of this interaction in the range between 0.7 and 1.0 eV depending on the orientation of the precursor with respect to the surface; Fig. 3 illustrates a typical configuration of a precursor atop the hydroxylated SiO_2 surface. The parameters of the effective interaction between oxygen atoms were derived to reproduce the boiling temperature of the O_2 gas, being equal to 90.2 K. The resulting parameters are summarized in Tab. 2.

	ε, kcal/mol	R_{min}, Å
W	-0.7914	1.62
Si	-0.3660	2.22
O	-0.1794	1.32
C	-0.1623	1.55
H	-0.0460	0.22

Table 2. Parameters of the effective interatomic interactions used in simulations. The interactions are modeled using the Lennard-Jones potential defined in [26]. The minimal energy of a pairwise interaction between atoms of type i and j is thus defined as $\varepsilon_{ij} = \sqrt{\varepsilon_i \varepsilon_j}$, while the equilibrium distance is $R_{min} = (R_{min_i} + R_{min_j})/2$.

4 Results

This section reports the results of computer simulations of the MD and IDMD processes introduced above. The results obtained are compared with the available experiments and thoroughly analysed.

4.1 Diffusion of $W(CO)_6$ atop hydroxylated SiO_2 surface

Let us consider first the results of simulations of diffusion of $W(CO)_6$ over the fixed hydroxilated SiO_2 surface. The diffusion process is simulated at different temperatures. The concept of temperature is applied to the atoms of precursor molecules; only these atoms are allowed to move, rotate and vibrate, and, therefore, we introduce temperature of this subsystem through the average kinetic energy of the atoms involved. The substrate is considered "frozen", i.e. static, such that its atoms do not move but create a force field for the precursor molecules to move in. Since this force field appears to act as an external field, it does not lead to any energy losses or cooling of the dynamical part of the system but allows us to study the diffusion

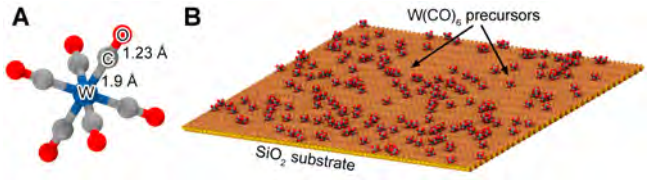

Fig. 4. Structure of a single tungsten hexacarbonyl $W(CO)_6$ molecule (A) as optimized using MBN Explorer. Precursor molecules are adsorbed on the hydroxilated SiO_2 surface (B) and experience diffusion behaviour in the absence of irradiation.

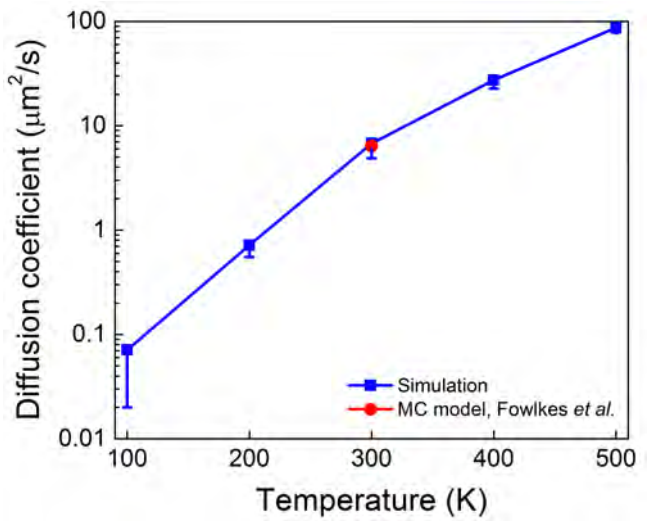

Fig. 5. Comparison of the simulated diffusion coefficient (blue curve) with the value obtained in [56] within the MC modelling approach (red dot). The match of the diffusion coefficients validates the sufficiently accurate description of the interaction between precursor molecules and the surface.

process with correct efficient interaction of the precursor molecules and the surface.

First of all the initial structure of $W(CO)_6$ molecule has been optimized using the steepest descent optimisation algorithm implemented in MBN Explorer and found to be in a good agreement with the structure described in the NIST database[6], see Fig. 4A.

Then, the diffusion process of precursors over the hydroxilated SiO_2 surface has been simulated, see Fig. 4B, using the methodology described in [63]. The obtained diffusion coefficients are compared to those estimated in [56] and a good agreement with the results reported in that work has been established. Figure 5 shows the dependence of the simulated surface diffusion coefficient on temperature. The red dot corresponds to the value obtained by Fowlkes *et al.* [56] within the MC modelling approach. At the room temperature the simulated diffusion coefficient value is 6.77 $\mu m^2/s$. This number is 5% different from the respective number 6.4 $\mu m^2/s$ reported earlier [56].

[6] http://webbook.nist.gov/cgi/cbook.cgi?ID=C14040110

The results obtained indicate that the utilised force field provides a good description of the equilibrium geometry of $W(CO)_6$ and its interaction with the surface.

4.2 Adsorption and irradiation of precursor molecules

Let us now discuss IDMD simulations of the adsorption and irradiation of precursors on the surface in the course of the FEBID process performed at different values of the electron beam current. The IDMD simulations demonstrate the formation of molecular fragments and their merging into an island, i.e. the W-enriched molecular structure atop the SiO_2 surface. The process of the island growth is characterized and analyzed.

Figure 6A shows the time dependence of the size of the largest W enriched island emerged in simulations of the FEBID process with the parameters corresponding to the reference case study described above. Figures 6B, 6C, 6D show the same for the number of W atoms, the number of $W(CO)_6$ and CO molecules in the system, respectively. The replenishment phases are excluded from the plots in Fig. 6. The drops in the number of CO molecules (Fig. 6D) and the jumps in the number of $W(CO)_6$ (Fig. 6C) arise each 10 ns, i.e. at the beginning of each new irradiation run. Both the size and the number of W atoms in the W enriched islands grow because new atoms are being attached to the islands during the FEBID process. To characterize this process an island with the maximum size has been selected on each step and the number of atoms in it is plotted in Figs. 6A. Figure 6B shows the number of W atoms in the island. These dependencies indicate the coalescence of smaller islands into a larger single nanostructure (ripening process) during the initial stage of the FEBID process. The irregular spikes on the curves arise at the instants when separate islands merge together.

The $W-(CO)$ bonds in precursors dissociate during the irradiation phase and separate CO molecules emerge. Most of the CO molecules are created in the vicinity of the surface and later evaporated into the vacuum chamber. The evaporation process continues during the replenishment phases. Figure 6 shows the time evolution of the number of CO molecules attached to the SiO_2 surface. It is seen that during each irradiation phase the number of CO molecules nonlinearly increases. To account for the evaporation process of CO during the replenishment phase, the CO molecules are removed from the simulation box volume after each irradiation phase. This leads to the abrupt decrease in the number of CO molecules every 10 ns, as seen in Fig. 6D. In Fig. 6A the number of electrons targeting the surface, i.e. the electron fluence, is indicated for the reference case study.

It is easy to rescale the simulation results presented in Figs. 6A-D to realistic experimental conditions. For this it is necessary to calculate the parameter λ, being the ratio of the experimental dwell time to the one used in simulations:

$$\lambda = \frac{\tau_d^{exp}}{\tau_d^{sim}}. \quad (3)$$

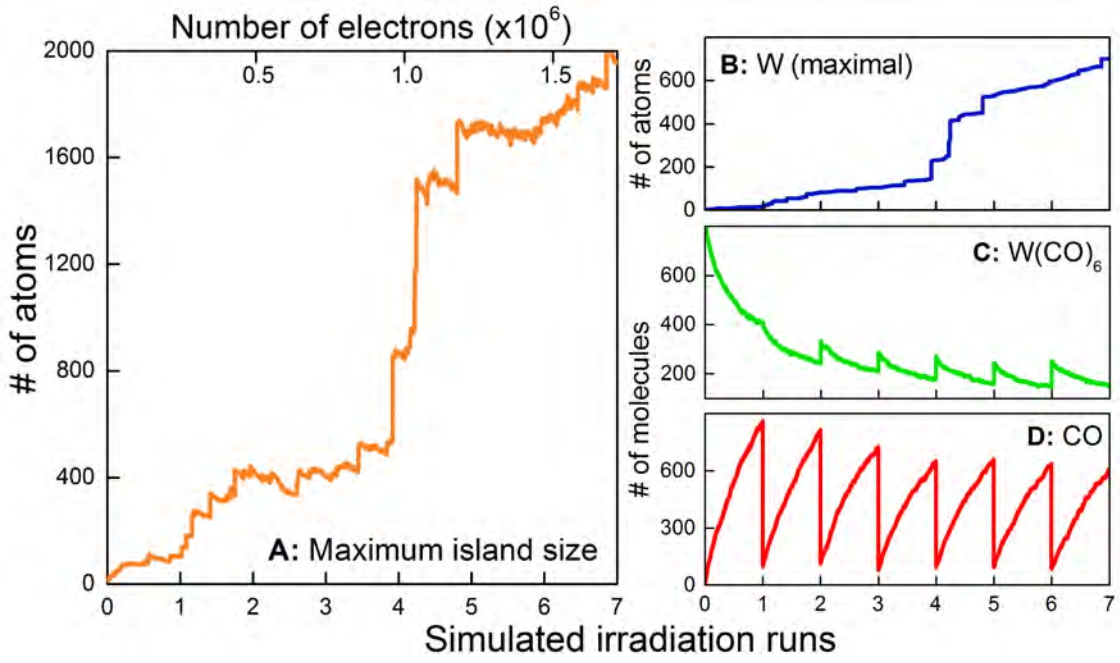

Fig. 6. Time evolution of the size of the largest W enriched island (A), the number of its constituent W atoms (B), the number of $W(CO)_6$ (C) and CO (D) molecules in the system in the course of simulation. The simulation consists of seven successive runs of irradiation (10 ns each) and adsorption as described in the text. Parameters if the system correspond to the reference case study.

Then, for a given electron beam radius R ($R = 5$ nm in the case presented in Fig. 6), the experimental electron beam current corresponding to the simulations can be evaluated as $I^{exp} = I^{sim}/\lambda$. Thus, for $\lambda = 10^5$, $\tau_d^{sim} = 10$ ns and $I^{sim} = 4$ μA, one derives $\tau_d^{exp} = 1$ ms and $I^{exp} = 40$ pA.

In general, the correspondence of simulated results to experimental ones can be established through the correspondence of the electron fluence per dwell time per unit area in simulations and experiment. In this case adsorbed precursors are exposed to the same irradiation conditions in both simulations and experiment. It is easy to see that this correspondence condition gives

$$I^{exp} = I^{sim}\frac{S^{exp}}{\lambda S^{sim}} = I^{sim}\frac{R^{exp^2}}{\lambda R^{sim^2}} \qquad (4)$$

where S^{exp} and S^{sim} is the electron beam cross section used in experiment and simulations. Thus, considering the experimental electron beam radius R^{exp} twice as big as R^{sim}, in the above considered example one derives $I^{exp} =$ 160 pA.

Finally, let us note again the outcome of irradiation at a given e-beam radius and current depends also on the e-voltage, which influences the electron induced dissociation cross section as seen from Eq. (1).

4.3 Nanostructure growth and its characterisation

Let us now demonstrate that the morphology, the type of emerging surface nanostructure and its composition depend strongly on the irradiation driven chemistry of precursors. For this purpose let us consider the models A and B introduced above. In both models, for the atoms with open bonds the algorithm of searching for the atomic open bond neighbours of the suitable type is implemented. In the case of model A the searching for the reactive neighbours is performed only among the atoms located beyond the molecular structure to which a chosen atom belongs. In the model B the search is performed over all open valence atoms in the system including the molecular structure to which a chosen atom belongs.

The nanostructures presented in Fig. 7 and Fig. 8 emerge after 150 ns of simulated irradiation (15 rounds of irradiation 10 ns each at the conditions corresponding to the e-beam current 1.2 μA, see above). These figures show that the chained structures of W (blue dots) with the C-O fragments attached to the most of W atoms are formed within model A, while model B results in the formation of more compact and dense molecular structure with the larger W content. The relative content of tungsten in these nanostructures is $\sim 15\%$ (model A) and $\sim 46\%$ (model B). These simulations also indicate that formation of chemical bonds within the growing nanostructure is essential for the emergence of the crystalline-like molecular structure with higher content of tungsten atoms. The increase of the number of bonds between W atoms leads to the decrease of the CO content and the total number of atoms in the growing nanostructure, i.e. its growth rate.

Figure 9 shows the dependence of W enriched nanostructure size and W content on irradiation time simulated for different values of irradiation intensity within the models A and B. One can notice that in the case of model B the size of the nanostructure is several times smaller while

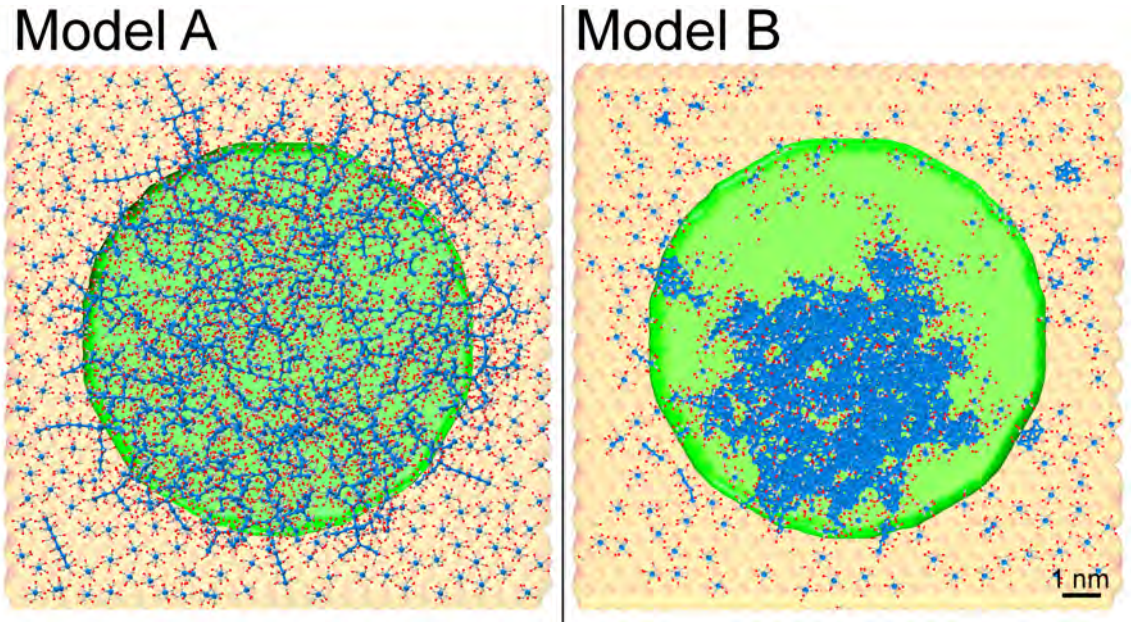

Fig. 7. Top view of morphologies of W enriched nanostructures atop the hydroxylated SiO_2 surface simulated within models A and B after 15 irradiation/adsorption cycles.

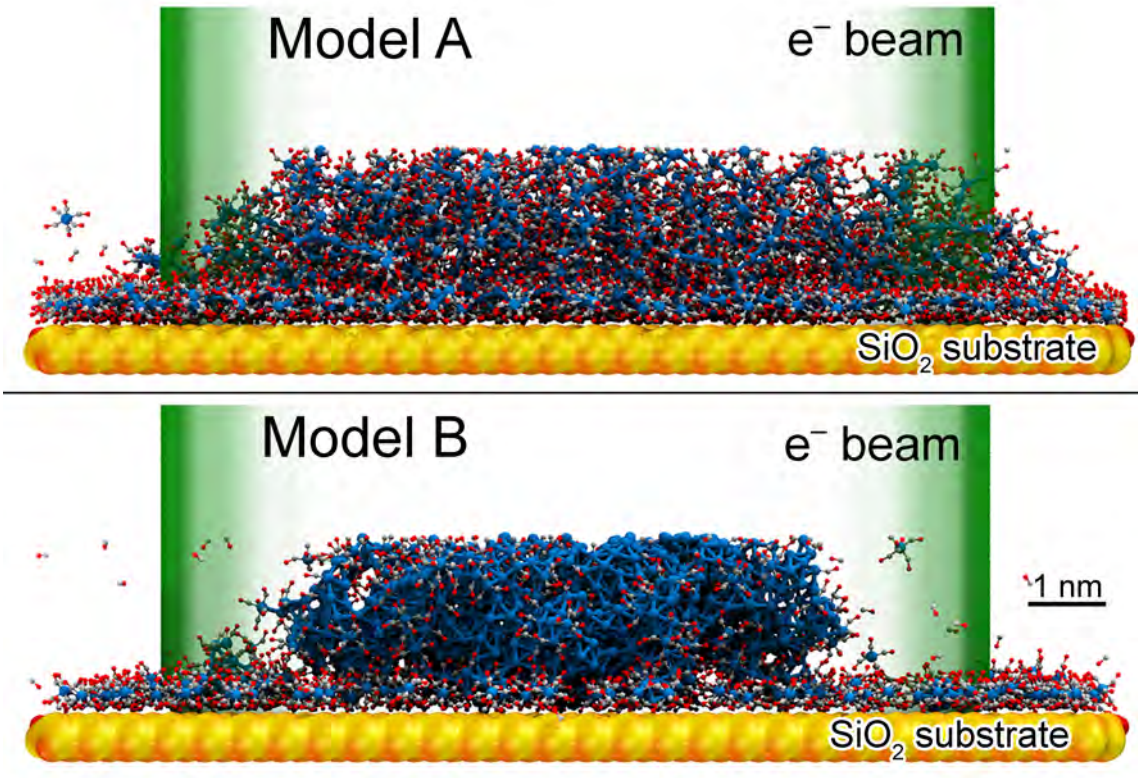

Fig. 8. Side view of morphologies of W enriched nanostructures shown in Fig. 7.

the W content is significantly higher. In both models the nanostructure growth rate and W content in the nanostructure after ~ 100 - 150 ns of simulated irradiation (depending on the electron beam current) fluctuates around constant values, although the island ripening process in the model B is not yet finished as evidenced by jumps in the dependence of the island size on irradiation time. It is also seen from Figs. 7 and 8 that merging of separate islands in model B is still possible.

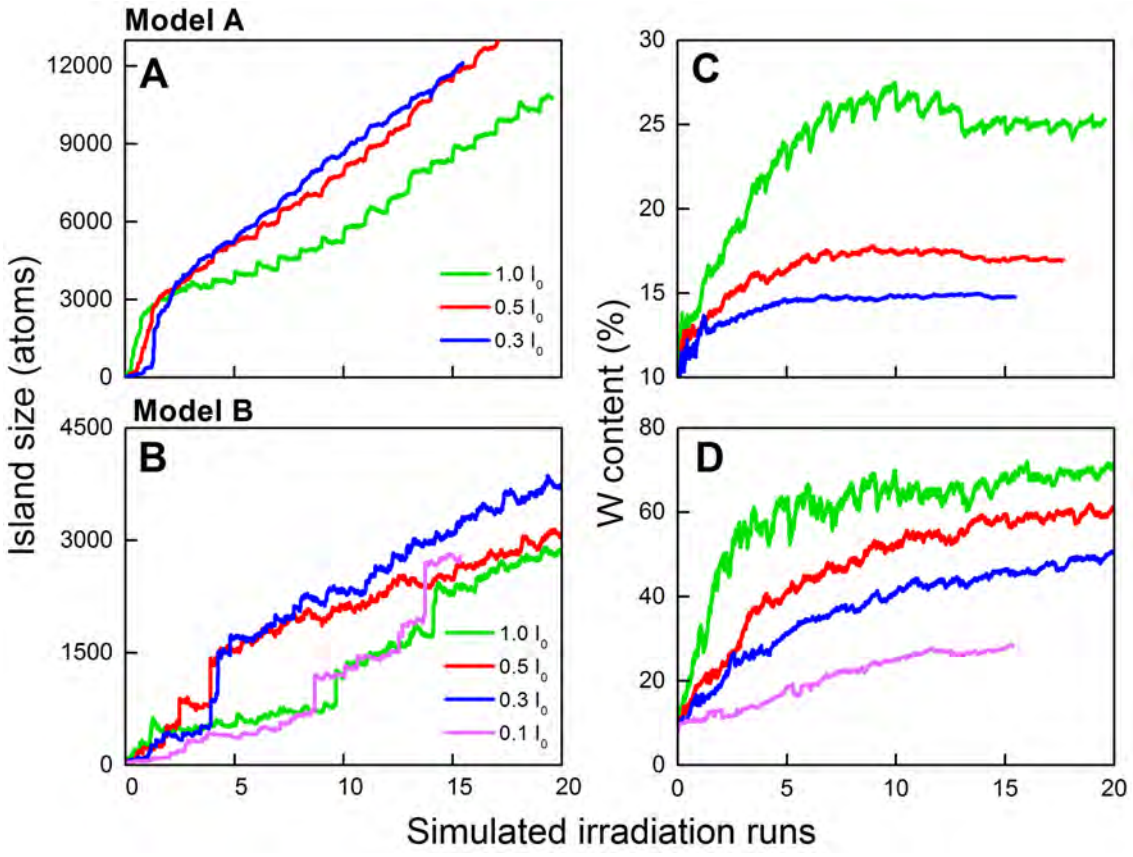

Fig. 9. Time evolution of W enriched nanostructure size and W content simulated at different intensities of the electron beam for models A and B. I_0 is equal to 4 μA, all other simulation parameters correspond to the reference case study.

	Beam current / acc. voltage / τ_d (Amp/keV/ns)	Fluence e^-/τ_d e^-/fs	Fluence $e^-/\tau_d \pi R^2$ e^-/(fs nm^2)	Vol. growth rate (nm^3/e^-) $\times 10^{-5}$	W content (%)
Simulation model A	$4.0{\cdot}10^{-6}$/30/10	$2.5{\cdot}10^5$	3178	5.23	25.4
	$2.0{\cdot}10^{-6}$/30/10	$1.2{\cdot}10^5$	1589	13.9	17.2
	$1.2{\cdot}10^{-6}$/30/10	$7.5{\cdot}10^4$	953	24.0	14.8
Simulation model B	$4.0{\cdot}10^{-6}$/30/10	$2.5{\cdot}10^5$	3178	1.22	67.0
	$2.0{\cdot}10^{-6}$/30/10	$1.2{\cdot}10^5$	1589	3.30	57.3
	$1.2{\cdot}10^{-6}$/30/10	$7.5{\cdot}10^4$	953	6.56	45.6
	$0.4{\cdot}10^{-6}$/30/10	$2.5{\cdot}10^4$	318	17.7	27.9
Exp. [56]	$79{\cdot}10^{-12}$/30/$1{\cdot}10^6$	$4.9{\cdot}10^5$	1569	6.33	
Fowlkes *et al.*	$25{\cdot}10^{-12}$/30/$1{\cdot}10^6$	$1.6{\cdot}10^5$	497	11.1	
Exp. [64]	$6.6{\cdot}10^{-9}$/5/$1{\cdot}10^5$	$4.1{\cdot}10^6$	13111		34.0
Huth *et al.*	$1.2{\cdot}10^{-9}$/5/$1{\cdot}10^5$	$7.5{\cdot}10^5$	2384		27.5

Table 3. Comparison of electron fluence, volume growth rates of the W enriched nanostructure, and W contents for different values of the electron beam current obtained for models A and B with experimental observations [56, 64].

The results of simulations are summarized in Tab. 3, where the average growth rates and the contents of W simulated within the models A and B at different electron beam currents are listed. These results are compared with the available experimental data. As discussed above, the results of simulations can be brought in correspondence to different experimental conditions according to the electron fluence per dwell time, per unit area. This characteristic is presented in Tab. 3 for both simulated and experimental case studies. In addition the total electron fluence per dwell time for all the cases considered is provided. To compare the results of simulations with experiment the volume growth rates and the W contents are presented in Tab. 3.

The e-current 2.0 μA in Models A and B corresponds to 79 pA in [56]. It is seen that the simulated volume growth rate in Model A overestimates the experimental value $6.33{\cdot}10^{-5}$ nm^3/e^- by approximately a factor of two, while the model B underestimates the volume growth rate

by approximately a factor of two (when evaluating the experimental volume growth rate the semi-ellipsoidal shape of the sample is assumed). These discrepancies indicate that the models require the further development, e.g. accounting for the dissociation of the C-O radicals. They can also be attributed to the manifestation of SE and BSE, which are accounted for in the models in a very simplistic way. The fluence per dwell time per unit area 497 $e^-/(fs\ nm^2)$ for the e-current 25 pA from [56] is in between the simulated values 318 $e^-/(fs\ nm^2)$ and 953 $e^-/(fs\ nm^2)$ within the model B. The experimental volume growth rate in this case is approximately equal to the average of the simulated volume growth rates in the aforementioned cases. The better agreement of the simulation result with experiment might be related to the use of the smaller e-currents and thus less influence of the SE and BSE effects.

The fluence per dwell time per unit area 2384 $e^-/(fs\ nm^2)$ for the e-current 1.2 nA from [64] is in between the simulated values 1589 $e^-/(fs\ nm^2)$ and 3178 $e^-/(fs\ nm^2)$ within both the models A and B. It is seen from Tab. 3 that the model A underestimates the experimental value by approximately 30%, but the model B overestimates it by more than two times. These discrepancies indicate the need of the further refinement of the models to better account for the irradiation driven chemistry. Thus, in experiments [64] the concentrations of carbon and oxygen in the resulting nanostructure significantly differ from each other. To reproduce this effect the dissociation of C-O bonds has to be taken into account. The dissociation energy of this type of bonds is much higher than for W-C bonds and their dissociation cannot be caused by purely thermal heating. The simulation involving irradiation driven dissociation of C-O bonds requires the probabilities for dissociation of this type of bonds which can be evaluated from the cross sections of the corresponding collision processes that are available in the literature and databases[7]. This will be the task for the further investigations. It is also worth to note that the e-voltage in the experiments [64] is 6 time smaller than those used in simulations. This might strongly affect the production of SE and BSE and thus contribute to the discrepancy between the simulated results and experiment. Another factor which might also play a role is the finite width of the experimental substrates.

The results demonstrate that the IDMD approach provides a powerful computational tool to model the growth process of W granular metal structures emerging in the FEBID process at the atomistic level of detail. The morphology of the simulated structures, their composition and growth characteristics are consistent with the available experimental data. Moreover, the observed dependencies like increasing of the volume growth rate per incident electron with decreasing the e-beam current, or the growth of the W content with increase of the e-beam current are reproduced correctly by within the developed models. The performed analysis indicates also the need of further advancements of the introduced methodology.

[7] vamdc.org

Let us mention possible refinements of the modeling approach which can be explored in the future. The Lennard-Jones potential for the interaction between tungsten atoms describes the major characteristics of the metallic structure such as density and the binding energy of atoms. The more accurate description of metallic structures, clusters or nanoparticles with crystalline structure should be performed with EAM-like potentials (EAM-Embedded Atom Method) such as Finnis-Sinclair [65] or Sutton-Chen [66] potentials, which are widely used for metals and which are implemented in MBN Explorer.

The employed models for the IDMD simulations of the FEBID process can, therefore, be refined through (i) the utilisation of the EAM-like force field for the description of interaction between W atoms, (ii) accounting for the CO bonds dissociation and (iii) considering the non-uniform distribution of SE and BSE and related probability of bond dissociation.

The further work in the direction will aim to describe in greater detail the system state in the simulation box corresponding to the one which arises in the vicinity of the surface in the FEBID experiments. This will require to further adopt the model to the actual adsorption conditions, to improve the set of parameters for the electron-precursor interaction, to extend the model for other types of precursors, e.g $(CH_3)CpCH_3Pt$, $HFCo_3(CO)$, Si_5H_{12} and $Co_2(CO)_8$, to extend the simulation time in order to model formation of larger crystalline structures, thermal effects and possible phase transitions there.

The newly introduced methodology based on the IDMD should be capable to capture the main features of the FEBID process at the atomistic level of detail and to provide the quantitative description of the radiation driven surface nanostructure formation for different parameters of electron beams, precursors, adsorption conditions and the related chemistry, surface properties, as well as to account for the thermal effects in the system.

5 Conclusions

The developed IDMD approach is suitable for computational modelling and analysis of irradiation driven chemical transformations of complex molecular systems. The approach accounts for irradiation induced quantum transformations in the system as random, fast and local processes involving small molecules or molecular fragments. It is demonstrated that the quantum transformations, such as molecular bond breaks, creation and annihilation of open valence bonds, changes in molecular topologies, etc, can be incorporated locally into the molecular force fields that describe the classical MD of complex molecular systems under irradiation.

The IDMD method is validated through simulations of the FEBID process of tungsten hexacarbonyl $W(CO)_6$ precursor molecules on the hydroxilated SiO_2 surface. It is demonstrated that knowing the interaction parameters for the fragments of the molecular system arising in the course of irradiation one can reproduce reasonably well experimental observations and make predictions about mor-

phologies of molecular structures that emerge on the surface in the FEBID process.

The introduced IDMD methodology opens a broad range of possibilities for the atomistic description and modelling of irradiation driven modifications and chemistry of complex molecular systems in many research areas ranging from radiotherapy cancer treatments to the emerging technologies such as FEBID in material science, plasma physics and other research areas in which irradiation of materials or complex molecular systems plays a role.

The IDMD approach is implemented into the MBN Explorer software package capable to operate with a large library of classical potentials, many-body force fields (including the recently implemented reactive CHARMM force field) and their various combinations. Therefore, it provides unique possibilities for the computational studies and modelling of the irradiation driven chemistry of the above mentioned systems.

As a concluding remark, we would like to note that the reactive force field employed by IDMD considers the motion of atoms within the framework of classical dynamics. We, thus, do not account for electronic excitations in the molecular fragments, assuming that all such excitations would relax significantly faster than most of the dynamical processes that are studied using IDMD, and are thus not expected to play significant role in the dynamics. The present realization of IDMD does not permit to analyze how the vibrational energies are redistributed in fragments upon bond rapture. This could be a potential further extension of the model that may be included in the next release of the IDMD method. However, we advocate that even if the redistribution of vibrational energies upon bond rupture is present, this effect should not be of large importance in the considered problem, because of the presence of temperature control. The temperature control leads to thermalizing of the system on times that are significantly shorter than the simulation times, and, therefore, all vibrational excitations would be thermalized fast.

Another limitation of the present model is that it does not explicitly account for charge delocalization or redistribution effects. Irradiation-induced charge effects on the surface could significantly change the mobility and desorption of some ionic fragments. Some of these effects are accounted for empirically as we take corrections for the current of surface electrons. We also put empirically how many molecules remain on the surface after desorption, which allows at least qualitatively to account for some of the effects mentioned. Including charge effects into the simulation would be a routine procedure after further modifications of MBN Explorer code. It is, however, expected that modification would make the calculations much more involved and computer time demanding. Following this reasoning we, therefore, believe that such an extension of the model should not be a part of the present work as it already contains a significant amount of novel and original results, and including further algorithm extensions would be much better received if placed in a separate publication.

6 Acknowledgments

We thank Michael Huth for useful discussions and suggestions on the experimental aspects of the FEBID process. The possibility to perform computer simulations at the DeiC National HPC Center, SDU is gratefully acknowledged. IAS is grateful for the financial support from the Lundbeck Foundation, and to the Russian Scientific Foundation (Grant No. 14-12-00342). GBS is grateful for the financial support from COST Action CM1301 (CELINA).

References

1. D. Schardt, T. Elsässer, D. Schulz-Ertner, Reviews of modern physics **82**(1), 383 (2010)
2. E. Surdutovich, A.V. Solovyov, The European Physical Journal D **66**(8), 1 (2012)
3. A.G.G.M. Tielens, Rev. Mod. Phys. **85**, 1021 (2013), `http://link.aps.org/doi/10.1103/RevModPhys.85.1021`
4. G. Horneck, C. Baumstark-Khan, eds., *Astrobiology: The Quest for the Conditions of Life* (Springer-Verlag Berlin Heidelberg, 2002), ISBN 978-3-642-59381-9
5. M. Huth, F. Porrati, C. Schwalb, M. Winhold, R. Sachser, M. Dukic, J. Adams, G. Fantner, Beilstein journal of nanotechnology **3**(1), 597 (2012)
6. I. Utke, P. Hoffmann, J. Melngailis, Journal of Vacuum Science & Technology B **26**(4) (2008)
7. B. Wu, A. Kumar, Journal of Vacuum Science & Technology B **25**(6) (2007)
8. A.M. Hawryluk, L.G. Seppala, Journal of Vacuum Science & Technology B **6**(6), 2162 (1988)
9. F. Heidet, N.R. Brown, M. Haj Tahar, Reviews of Accelerator Science and Technology **8**, 99 (2015)
10. P. Dinh, P.G. Reinhard, E. Suraud, Phys. Rep. **485**, 43 (2010)
11. J. Maruhn, P. Reinhard, E. Suraud, *Simple Models of Many-Fermion Systems* (Springer-Verlag Berlin Heidelberg, 2010)
12. D. Jacquemin, V. Wathelet, E.A. Perpéte, C. Adamo, Journal of Chemical Theory and Computation **5**(9), 2420 (2009)
13. A.D. Bochevarov, E. Harder, T.F. Hughes, J.R. Greenwood, D.A. Braden, D.M. Philipp, D. Rinaldo, M.D. Halls, J. Zhang, R.A. Friesner, International Journal of Quantum Chemistry **113**(18), 2110 (2013)
14. P. Husen, I.A. Solovyov, Journal of the American Chemical Society (2016)
15. K. Sanbonmatsu, C.S. Tung, J. Struct. Biol. **157**, 470 (2007)
16. G. Zhao, J.R. Perilla, E.L. Yufenyuy, X. Meng, B. Chen, J. Ning, J. Ahn, A.M. Gronenborn, K. Schulten, C. Aiken et al., Nature **497**, 643 (2013)
17. A.C. Pan, T.M. Weinreich, S. Piana, D.E. Shaw, Journal of Chemical Theory and Computation **12**(3), 1360 (2016)
18. R. Salomon-Ferrer, A.W. Gotz, D. Poole, S. Le Grand, R.C. Walker, J. Chem. Theory Comput. **9**, 3878 (2013)

19. A.K. Rappé, C.J. Casewit, *Molecular mechanics across chemistry* (University Science Books, 1997)
20. J. Gumbart, E. Schreiner, D.N. Wilson, R. Beckmann, K. Schulten, Biophys. J. **103**, 331 (2012)
21. J. Shim, G.I. Humphreys, B.M. Venkatesan, J.M. Munz, X. Zou, C. Sathe, K. Schulten, F. Kosari, A.M. Nardulli, G. Vasmatzis et al., Sci. Rep. **3**, 1389 (2013)
22. E. Sjulstok, J.M.H. Olsen, I.A. Solov'yov, Scientific Reports **5**, 18446 (2015)
23. G. Lüdemann, I.A. Solov'yov, T. Kubař, M. Elstner, Journal of the American Chemical Society **137**, 1147 (2015)
24. B. Brooks, R. Bruccoleri, B. Olafson, D. States, S. Swaminathan, M. Karplus, J. Comp. Chem. **4**, 187 (1983)
25. D.A. Case, T.E. Cheatham, T. Darden, H. Gohlke, R. Luo, K.M. Merz, A. Onufriev, C. Simmerling, B. Wang, R.J. Woods, J. Comp. Chem. **26**, 1668 (2005)
26. D.V.D. Spoel, E. Lindahl, B. Hess, G. Groenhof, A. Mark, H. Berendsen, J. Comp. Chem. **26**, 1701 (2005)
27. J.C. Phillips, R. Braun, W. Wang, J. Gumbart, E. Tajkhorshid, E. Villa, C. Chipot, R.D. Skeel, L. Kale, K. Schulten, J. Comp. Chem. **26**, 1781 (2005)
28. I.A. Solov'yov, A.V. Yakubovich, P.V. Nikolaev, I. Volkovets, A.V. Solov'yov, Journal of Computational Chemistry **33**, 2412 (2012)
29. G.B. Sushko, I.A. Solov'yov, A.V. Verkhovtsev, S.N. Volkov, A.V. Solov'yov, European Physical Journal D **70**, 1 (2016)
30. I.A. Solov'yov, G.B. Sushko, A.V. Verkhovtsev, A.V. Korol, A.V. Solov'yov, *MBN Explorer: Dynamics of Biomolecular Systems and Self-organization* (Polytechnic University Publishing House, St. Petersburg State Polytechnic University, St. Petersburg, Russia, 2015), ISBN 978-5-7422-4894-1
31. I.A. Solov'yov, G.B. Sushko, A.V. Verkhovtsev, A.V. Korol, A.V. Solov'yov, *MBN Explorer: Simulations of Nanomaterials Structure and Dynamics* (Polytechnic University Publishing House, St. Petersburg State Polytechnic University, St. Petersburg, Russia, 2015), ISBN 978-5-7422-4893-4
32. V.V. Dick, I.A. Solov'yov, A.V. Solov'yov, Physical Review B **84**, 115408 (2011)
33. V.V. Dick, I.A. Solov'yov, A.V. Solov'yov, *Nanoparticles dynamics on a surface: fractal pattern formation and fragmentation* (2010), Vol. 248, pp. 012025–(1–11)
34. M. Panshenskov, I.A. Solov'yov, A.V. Solov'yov, Journal of Computational Chemistry **35**, 1317 (2014)
35. I.A. Solov'yov, A.V. Solov'yov, N. Kébaili, A. Masson, C. Bréchignac, Physica Status Solidi B **251**, 609 (2014)
36. I.A. Solov'yov, A.V. Solov'yov, *Simulation of nanofractal dynamics with MBN Explorer* (2013), Vol. 438, pp. 012006–(1–12)
37. G.B. Sushko, V.G. Bezchastnov, I.A. Solov'yov, A.V. Korol, W. Greiner, A.V. Solov'yov, Journal of Computational Physics **252**, 404 (2013)
38. G. Sushko, A. Korol, W. Greiner, A. Solov'yov, J. Phys. Conf. Ser. **438**, 012018 (2013)
39. G. Sushko, V. Bezchastnov, A. Korol, W. Greiner, A. Solov'yov, R. Polozkov, V. Ivanov, J. Phys. Conf. Ser. **438**, 012019 (2013)
40. G.B. Sushko, A.V. Korol, A.V. Solovyov, Nucl. Instr. Meth. Phys. Res. B **355**, 39 (2015)
41. A.V. Verkhovtsev, S. Schramm, A.V. Solovyov, Eur. Phys. J. D **68**, 246 (2014)
42. A.V. Verkhovtsev, M. Hanauske, A.V. Yakubovich, A.V. Solovyov, Comput. Mater. Sci. **76**, 80 (2013)
43. G.B. Sushko, A.V. Verkhovtsev, A.V. Solovyov, J. Phys. Chem. A **118**, 8426 (2014)
44. I.A. Solov'yov, M. Mathew, A.V. Solov'yov, W. Greiner, Physical Review E **78**, 051601 (2008)
45. J. Geng, I.A. Solov'yov, D.G. Reid, P. Skelton, A.E.H. Wheatley, A.V. Solov'yov, B.F.G. Johnson, Physical Review B **81**, 214114 (2010)
46. J. Geng, I.A. Solov'yov, W. Zhou, A.V. Solov'yov, B.F.G. Johnson, The Journal of Physical Chemistry C **113**, 6390 (2009)
47. I.A. Solov'yov, J. Geng, A.V. Solov'yov, B.F. Johnson, Chemical Physics Letters **472**, 166 (2009)
48. P. Moskovkin, M. Panshenskov, S. Lucas, A.V. Solov'yov, Phys. Status Solidi B **251**, 1456 (2014)
49. G.B. Sushko, A.V. Verkhovtsev, A.V. Yakubovich, S. Schramm, A.V. Solovyov, J. Phys. Chem. A **118**, 6685 (2014)
50. A.V. Verkhovtsev, A.V. Yakubovich, G.B. Sushko, M. Hanauske, A.V. Solovyov, Comput. Mater. Sci. **76**, 20 (2013)
51. A.V. Yakubovich, E. Surdutovich, A.V. Solov'yov, J. Phys.: Conf. Ser. **373**, 012014 (2012)
52. E. Surdutovich, A.V. Yakubovich, A.V. Solov'yov, Eur. Phys. J. D **60**, 101 (2010)
53. E. Surdutovich, A.V. Yakubovich, A.V. Solov'yov, Sci. Rep. **3**, 1289 (2013)
54. E. Surdutovich, A.V. Solovyov, The European Physical Journal D **68**(11), 1 (2014)
55. K. Vanommeslaeghe, E. Hatcher, C. Acharya, S. Kundu, S. Zhong, J. Shim, E. Darian, O. Guvench, P. Lopes, I. Vorobyov et al., J. Comput. Chem. **31**, 671 (2010)
56. R.B. Best, X. Zhu, J. Shim, P.E.M. Lopes, J. Mittal, M. Feig, A.D. MacKerell, J. Chem. Theory Comput. **8**, 3257 (2012)
57. A.D. MacKerell, Jr., D. Bashford, M. Bellott, R.L. Dunbrack, Jr., J.D. Evanseck, M.J. Field, S. Fischer, J. Gao, H. Guo, S. Ha et al., J. Phys. Chem. B **102**, 3586 (1998)
58. J.D. Fowlkes, P.D. Rack, ACS nano **4**(3), 1619 (2010)
59. A.M. Barragan, A.R. Crofts, K. Schulten, I.A. Solov'yov, Jeurnal of Physical Chemistry B **119**, 433 (2015)
60. E. Fermi, J. Pasta, S. Ulam, *Studies of nonlinear problems*, Los Alamos report LA-1940 (1955)
61. N. Silvis-Cividjian, C. Hagen, L. Leunissen, P. Kruit, Microelectronic engineering **61**, 693 (2002)
62. F. Salvat-Pujol, H.O. Jeschke, R. Valentí, Beilstein journal of nanotechnology **4**(1), 781 (2013)
63. G. Cetini, O. Gambino, Accad. Sci. Torino., Classe Sci. Fis. Mat. Nat., **1197** (1963)
64. K. Muthukumar, I. Opahle, J. Shen, H.O. Jeschke, R. Valentí, Physical Review B **84**(20), 205442 (2011)
65. A.V. Yakubovich, A.V. Verkhovtsev, M. Hanauske, A.V. Solovyov, Comput. Mater. Sci. **76**, 60 (2013)
66. M. Huth, D. Klingenberger, C. Grimm, F. Porrati, R. Sachser, New Journal of Physics **11**(3), 033032 (2009)
67. M. Finnis, J. Sinclair, Philosophical Magazine A **50**(1), 45 (1984)
68. A.P. Sutton, J. Chen, Philos. Mag. Lett. **61**, 139 (1990)